Journal of Power Sources 195 (2010) 1190–1194

Contents lists available at ScienceDirect

Journal of Power Sources

journal homepage: www.elsevier.com/locate/jpowsour

Short communication

Hydrogen desorption properties of Mg thin films at room temperature

Jianglan Qu[a], Bo Sun[b], Jie Zheng[a], Rong Yang[a], Yuntao Wang[a], Xingguo Li[a,b,*]

[a] Beijing National Laboratory for Molecular Sciences (BNLMS), The State Key Laboratory of Rare Earth Materials Chemistry and Applications, College of Chemistry and Molecular Engineering, Peking University, Beijing 100871, China
[b] College of Engineering, Peking University, Beijing 100871, China

ARTICLE INFO

Article history:
Received 29 March 2009
Received in revised form 25 August 2009
Accepted 25 August 2009
Available online 1 September 2009

Keywords:
Hydrogen storage
Magnesium thin films
Hydrogen desorption

ABSTRACT

Pd–Mg–Pd thin films prepared by magnetron sputtering could absorb hydrogen entirely at room temperature and dehydrogenate completely and rapidly in ambient air. Our investigations of the structural, optical and electrical properties gave a detailed insight into the desorption mechanism. The overall activation energy and the hydrogen diffusion coefficient were deduced to be 48 kJ mol^{-1} and 8.0 × 10^{-15} cm^2 s^{-1} based on optical and electrochemical measurements, respectively. The desorption process followed the nucleation and growth mechanism by modeling and simulating the resistance data. The small activation energy and remarkable diffusion kinetics highlighted the applicability as on-board hydrogen storage systems.

1. Introduction

Hydrogen storage materials have attracted intensive attention for the future clean energy system. Mg has been considered among the most promising candidates for automotive applications due to its low cost, lightweight and high capacity (7.6 wt.% of hydrogen) [1]. However, the application is primarily limited by the high desorption temperature and slow kinetics. Recently, tremendous efforts have been devoted to decrease the operation temperature and improve the kinetics by preparing Mg-based nano-composites, utilizing their high chemical activity and short diffusion paths [2]. Energetic ball milling and cold rolling resulted in improved hydrogen storage properties due to increased surface area, formation of nanostructures and creation of defects [3,4]. Thin films offer a unique opportunity to carry out such studies as their composition, interface and crystallinity can be well tailored in nano-scales [5]. Therefore, Mg-based thin films achieved faster kinetics at lower temperature and hydrogen pressures compared with bulk Mg–Pd materials. Thus, various attempts have been undertaken to study the hydrogen storage properties of Mg thin films [6–9]. Designing of favorable structures, such as sandwich-like structured films, is an important strategy to achieve advantageous kinetics [10,11]. The cooperative phenomenon and spillover effect in this system might lead to the significant improvement in absorption kinetics [12]. Though the hydrogen absorption properties of Mg films have been the subjects of much study, the desorption behavior requires clarification. Some evidence indicated that smaller grain size, lower crystallinity, or doping with catalysts improved desorption kinetics in vacuum [13–16]. However, desorption behaviors of Mg films at moderate conditions need more discussions. Therefore, investigation of the corresponding kinetic parameters is of guidance to explore advanced Mg-based hydrogen storage materials.

Moreover, Mg-based thin films have been extensively studied as "switchable mirrors", which exhibit reversible and drastic optical changes upon hydrogen absorption and desorption [17–20]. As a result, Mg films could potentially be applied as hydrogen sensors, energy efficient windows and solar absorbers [21–24]. In this context, it is beneficial to design Mg films to improve the kinetics and lower the desorption temperature for their potential applications. Herein, we investigated the hydrogen desorption properties of sandwich-like Pd–Mg–Pd thin films at ambient air, by monitoring the structural, optical and electrical changes.

2. Experimental

Pd–Mg–Pd thin films were prepared by a custom designed direct current (DC) magnetron sputtering system with a background pressure of around 2 × 10^{-4} Pa. First, a 5 nm Pd layer was deposited onto Si (1 0 0) wafers, glass and ITO-coated (indium tin oxide) glass substrates by DC sputtering using a Pd (99.99%) target. The discharge power was 45 W and the argon (99.99%) pressure was 0.8 Pa. Then a 100 nm Mg layer was deposited on the Pd layer. The discharge power was 50 W and the argon pressure was 0.8 Pa. Finally, another 5 nm Pd layer was coated on top of the Mg layer by DC sput-

* Corresponding author at: Beijing National Laboratory for Molecular Sciences (BNLMS), The State Key Laboratory of Rare Earth Materials Chemistry and Applications, College of Chemistry and Molecular Engineering, Peking University, Beijing 100871, China. Tel.: +86 10 62765930; fax: +86 10 62765930.
E-mail address: xgli@pku.edu.cn (X. Li).

0378-7753/$ – see front matter © 2009 Elsevier B.V. All rights reserved.
doi:10.1016/j.jpowsour.2009.08.069

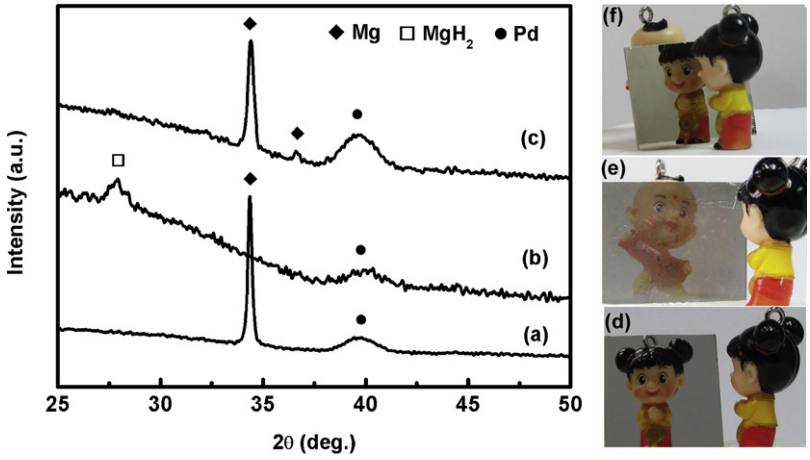

Fig. 1. XRD patterns of Pd–Mg–Pd thin films: (a) as-prepared; (b) after hydrogenation at 4×10^3 Pa H_2 at 298 K; (c) after dehydrogenation in air at 298 K. The photographs of Mg thin films: (d) as-prepared; (e) after hydrogenation; (f) after dehydrogenation.

tering, which is necessary to protect Mg against oxidation and to promote hydrogen dissociation. The deposition rates of Mg and Pd were 0.26 nm s^{-1} and 0.33 nm s^{-1}, respectively. After deposition, the samples were hydrogenated at 4×10^3 Pa hydrogen (99.99%) at room temperature for 4 h. The dehydrogenation process was performed in dry air at different temperatures for tracing desorption mechanism.

The structures of the samples were studied by powder X-ray diffraction (XRD) (Rigaku D/max-200) using monochromated Cu Kα radiation and $\theta - 2\theta$ scan. The film thickness was determined by cross-section scanning electron microscopy (SEM) measurements (Hitachi S4800). Optical transmission measurements at 298 K were performed using a UV–vis recording spectrophotometer (Shimadzu UV-2401PC) with a dual beam measurement system. The UV–vis transmission spectra at higher temperatures were measured with a Shimadzu UV-3100 spectrometer. The changes in resistance were recorded in a gas loading cell equipped with a four-probe resistance measurement, monitored by a Keithley 2000 digital multimeter. The diffusion coefficient of the Mg films deposited on ITO-coated glass substrate was determined by the electrochemical multipotential steps method in 6 M KOH solution. Platinum foil and Hg/HgO were used as the counter and reference electrode, respectively. The fast rate (100 mV s^{-1}) cyclic voltammogram was applied to clean the surface prior to measurement. The Mg film electrode was firstly held at a cathodically polarized potential (−1.10 V vs. Hg/HgO) for 2 h and subsequently switched to an anodically polarized potential (−0.5 V vs. Hg/HgO) for another 2 h.

3. Results and discussion

3.1. Structural characterization

The XRD patterns of Pd–Mg–Pd thin films after hydrogen absorption and desorption are shown in Fig. 1. The as-prepared sample preferentially grew along the (0 0 2) direction, as indicated by the peak around 34.6°. The broad peak around 40.0° was attributed to Pd (111). Upon exposure to 4×10^3 Pa H_2 at room temperature, the Mg (0 0 2) peak disappeared and the MgH_2 (1 1 0) peak became significant. Subsequently dehydrogenated at 298 K in air, the Mg (0 0 2) peak reappeared and the sample transformed completely from rutile β-MgH_2 to h-Mg. The Mg (1 0 1) peak also appeared at 36.5°, suggesting that the preferential orientation of (0 0 2) direction was attenuated due to the dehydrogenation induced reconstruction. The corresponding photographs of the samples are also shown in Fig. 1. The image of the cartoon girl was reflected on the as-prepared metallic film. After fully hydrogenation at 298 K, the boy behind the sample was observed clearly through the transparent sample. Subsequently dehydrogenated at ambient air, the highly reflecting shiny film obstructed the view of the cartoon boy again.

3.2. Hydrogen desorption kinetics

3.2.1. Activation energy in hydrogen desorption

Optical transmittance changes of the hydride films at 500 nm, T/T_0, with respect to desorption time under different temperatures in air are plotted in Fig. 2, where T_0 is the maximum transmittance after fully hydrogenation. Exposure to air caused a transition from the transparent hydride state to the high reflecting metallic state by dehydrogenation, during which the transmittance gradually decreased. Since the slopes of the transmittance curves represented desorption rates, faster dehydrogenation kinetics at higher temperatures were observed in the figure. Heating the samples increased the unloading rates, probably due to the temperature dependence of the surface reactions and the hydrogen diffusion [25]. The entire unloading process at 338 K took only 20 min, while at 298 K approximately 300 min were needed. Therefore, the overall rate at 338 K was 15 times larger than that at room temperature. This tendency could be suitable for practical use in the energy efficient windows because we are willing to change the window from the transpar-

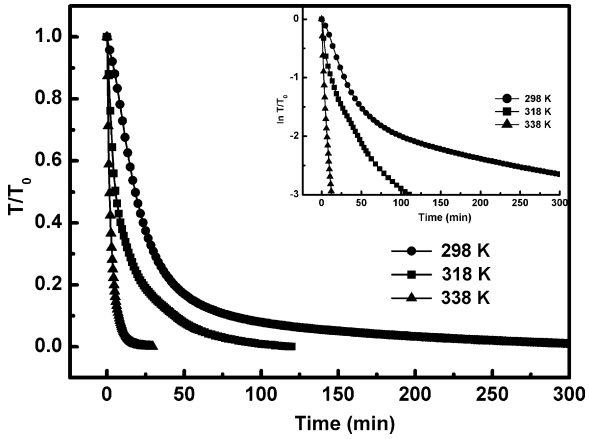

Fig. 2. Optical transmittance changes at 500 nm, T/T_0, with respect to desorption time under different temperatures in air. The inset is relative transmittance changes, $\ln T/T_0$, with respect to desorption time during dehydrogenation.

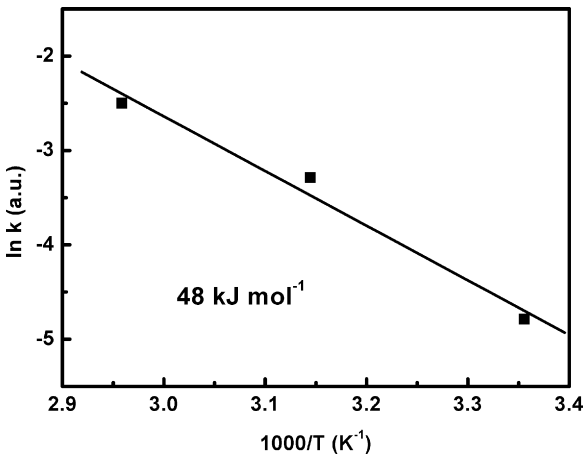

Fig. 3. Arrhenius plot of the desorption rate constants for hydrogen desorption in air. The straight line is the linear fit according to data.

ent state to the mirror state at hot condition to block sunshine [26].

According to the Lambert–Beer's law, $\ln(T/T_0)$, the logarithm of the optical transmission is expected to vary linearly with the hydrogen concentration in the film, as shown in Fig. 2 inset [27]. The desorption data had been analyzed using the Jonhnson–Mehl–Avrami theory [28]. Upon a first-order phase transition, the reacted fraction is given as function of time, by

$$r = 1 - \exp[-(kt)^n] \quad (1)$$

where r is the reacted fraction, t is the desorption time, $k = k(T)$ is the temperature dependent kinetic constant and n is the reaction order. A linear interpolation of the plots, $\ln(-\ln(1-r))$ versus $\ln(t)$, yielded the values of n and k. We used the transmittance data to calculate r, due to the reacted fractions of thin films were difficult to measure by the traditional gravimetric and volumetric method. Assuming that it was totally dehydrogenated when the transmittance kept constant as a function of time, it was then possible to determine the initial desorption rates from the slopes of the curves. Hence, the amount of hydride transforms to metal (reacted fraction r) in desorption process could be obtained. The value of the exponent was $n = 1$ for the desorption process [29]. The temperature dependent desorption rates generally followed the Arrhenius type law. The overall activation energy of hydrogen desorption was obtained as 48 kJ mol^{-1}, shown in Fig. 3. The activation energy was lower than the value 80 kJ mol^{-1} obtained in Mg–Pd system which we investigated before [30]. The smaller desorption activation energy could be attributed to the sandwich-like structure with Pd catalyst layers on both sides of the Mg layer. The cooperative interaction and the extended Pd–Mg interfaces were also favorable for the fast desorption at room temperature [15].

3.2.2. Electrical resistance

The time dependent resistance during hydrogen desorption provided information about the kinetic properties as well as hydrogen-induced changes of the electrical properties [31]. The time evolution of relative resistance changes, R/R_{max}, at different temperatures in air is shown in Fig. 4(a), where R_{max} is the initial resistance of the hydride film before dehydrogenation. The resistance decreased immediately upon exposure to air, due to the formation of metallic Mg grains during the dehydrogenation process. The resistance reached the similar value as that of the as-prepared film and did not change any more after a period of time, indicating that the samples completely transformed to metallic films. Therefore, the time needed for the resistance to saturate could be taken as an indicator of the average dehydrogenation rate.

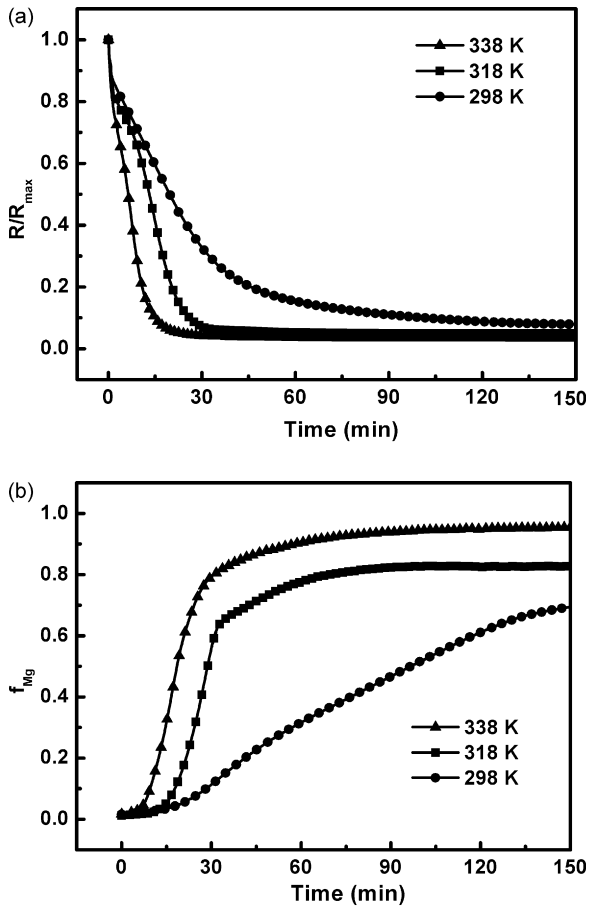

Fig. 4. (a) The relative resistance changes of Mg thin films during dehydrogenation in air at different temperatures. (b) The time dependent volume fraction of Mg during dehydrogenation in air at different temperatures.

As shown in the figure, the hydrogen desorption rates were much larger at higher temperatures. To analyze the hydrogen desorption kinetics in details, the volume fraction of Mg was calculated by fitting the resistance data. To simulate the experiments, we built a triple layer model with a 10 nm Pd layer in parallel with the Mg and MgH_2 layer. The changes in resistance were determined by the volume fraction of Mg. Mg had a resistivity of 6.5 μΩ cm and the resistivity of MgH_2 was assumed to be 10 mΩ cm. The time dependent volume fraction of Mg, f_{Mg}, is shown in inset Fig. 4(b). The data provided qualitative evidence that the desorption process underwent the nucleation and growth mechanism. First, few Mg nuclei might grow as isolated islands in the continuous MgH_2 film near the surface and the interface, leading to the sharp decrease in resistance and transmittance upon exposure to air [32]. Subsequently, more Mg nuclei rapidly formed and joined together and hydrogen atoms diffused through the growing metallic layer [33]. The second stage was an important factor governing desorption kinetics. Heating treatments accelerated desorption rates significantly during this period. At last, the nucleation rate slowed down and the film became metallic completely.

3.2.3. Hydrogen diffusion coefficient

Hydrogen diffusion coefficient was an important kinetics parameter. Hagi's model was applied to analyze the current with respect to the discharge time to calculate the hydrogen diffusion coefficient [34,35]. The current density could be approximated as

$$J_H = \frac{(C_0 - C^*)D_H}{L^2} \times \exp\left(\frac{-\pi^2 D_H t}{4L^2}\right) \quad (2)$$

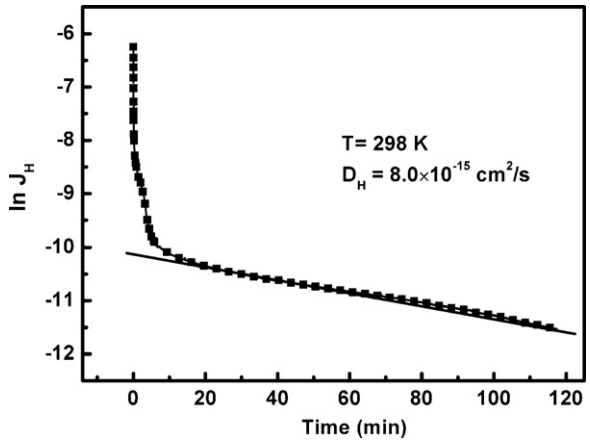

Fig. 5. Hydrogen diffusion coefficient of Mg thin films at room temperature. The straight line is the linear fit according to data.

where J_H is the current density, t is the discharge time, D_H is the diffusion coefficient, L is the thickness of the film electrode, C_0 is the initial hydrogen concentration, C^* is the hydrogen concentration after the electrode is anodically biased. Therefore, a plot of $\ln(J_H)$ with respect to the discharge time should be a straight line after a long time with the slope $-\pi^2 D_H t/4L^2$, thus the diffusion coefficient could be calculated in Fig. 5. The hydrogen diffusion coefficient at 298 K was deduced to be 8.0×10^{-15} cm^2 s^{-1}, which is larger than the value $D_H = 1.1 \times 10^{-16}$ cm^2 s^{-1} at 300 K [36]. The larger diffusion rate could be attributed to the favorable structure of the Mg films.

The kinetic response of the Mg film as a potential hydrogen sensor is illustrated in Fig. 6. Results show the switching cycles of the thin films by monitoring the changes in resistance, R/R_M, as a function of time, where R_M is the maximum resistance in the first cycle. We investigated the switching cycles of the samples at two desorption processes. These films were exposed to 4×10^3 Pa hydrogen first and then alternatively to air or vacuum at room temperature. In order to simplify the discussion about the response kinetics, we calculated the slopes of the initial changes in resistance as desorption kinetics parameters. These samples showed obviously faster desorption kinetics in air than vacuum. This was probably caused by the oxidation reactions on the Pd layer [25]. The equilibrium hydrogen pressure was calculated by means of the Van't Hoff equation. High thermodynamic stability of MgH_2 resulted in a relatively high desorption enthalpy, which corresponded to an unfavorable desorption temperature of 553 K at 10^5 Pa H_2. In addition, the slow

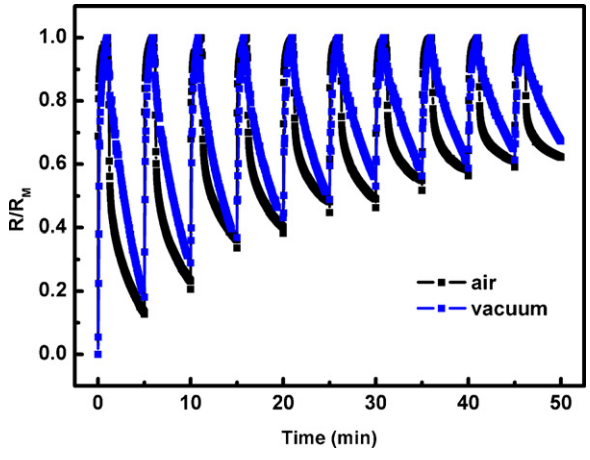

Fig. 6. Relative resistance changes, R/R_M, with respect to switching time in 4×10^3 Pa H_2 and air/vacuum at 298 K.

kinetics was a major impediment for its practical application at 298 K. However, the catalyst effect of Pd layer and nanocrystalline structure, as well as the oxidation reaction between the oxygen and the films, resulted in the faster absorption kinetics of Mg-based thin films at room temperature. The same degradation phenomenon was observed for both conditions, as well as other Mg-based systems. The formation of magnesium oxide at the outermost surface after repeated cycles was the reason for the degradation [37,38]. Other possible reasons could be that alloying between Mg and Pd during cycling resulted in the failure of the Pd cap layer and the non-reversible hydride formed [39,40]. The encapsulation of Pd catalysts was usually observed and caused by strong metal–support interaction (SMSI) [41]. No clear evidence for the formation of Mg–Pd alloy was observed. For instance, no interfacial Mg–Pd alloy seemed to be formed in Mg-based thin films during hydrogen absorption [8,11,15]. However, there might exist alloying over a few atomic layers at the interface. The formation of a very thin interface Mg–Pd alloy at most three-monolayer thick was found for Mg–Pd films after desorption at 468 K [42].

4. Conclusions

In summary, we demonstrated the hydrogen desorption properties of sandwich-like Pd–Mg–Pd films in air at room temperature. The samples became transparent and insulating after hydrogenation, and reverted to the metallic mirror state completely and rapidly on exposure to air at 298 K. The desorption process followed the nucleation and growth mechanism. The dehydrogenation rates increased at higher temperatures and the overall activation energy was 48 kJ mol^{-1}. The hydrogen diffusion coefficient was calculated as 8.0×10^{-15} cm^2 s^{-1} at 298 K. The small activation energy and fast diffusion rate were attributed to the cooperative interaction and extended interfaces. With the remarkable absorption and desorption kinetics, Mg-based films could be favorable candidates as hydrogen storage materials for fuel cell automobiles.

Acknowledgments

The authors acknowledge financial support from the National Natural Science Foundation of China (Nos. 20221101 and 20671004), MOST of China (Nos. 2006AA05Z130 and 2007AA05Z118) and MOE of China (No. 707002).

References

[1] A.Z.L. Schlapbach, Nature 414 (2001) 353–358.
[2] K.J. Jeon, A. Theodore, C.Y. Wu, J. Power Sources 183 (2008) 693–700.
[3] A. Zaluska, L. Zaluski, J.O. Strom-Olsen, J. Alloys Compd. 288 (1999) 217–225.
[4] J. Dufour, J. Huot, J. Alloys Compd. 439 (2007) L5–L7.
[5] R.D. Ferrer, M.G. Sridharan, G. Garcia, F. Pi, J. Rodriguez-Viejo, J. Power Sources 169 (2007) 117–122.
[6] J. Isidorsson, I.A.M.E. Giebels, H. Arwin, R. Griessen, Phys. Rev. B 68 (2003) 115112.
[7] K. Yoshimura, Y. Yamada, M. Okada, Surf. Sci. 566 (2004) 751–754.
[8] J. Paillier, S. Bouhtiyya, G.G. Ross, L. Roue, Thin Solid Films 500 (2006) 117–123.
[9] A. Leon, E.J. Knystautas, J. Huot, R. Schulz, J. Alloys Compd. 345 (2002) 158–166.
[10] K. Higuchi, K. Yamamoto, H. Kajioka, K. Toiyama, M. Honda, S. Orimo, H. Fujii, J. Alloys Compd. 330 (2002) 526–530.
[11] J. Rydén, B. Hjörvarsson, T. Ericsson, E. Karlsson, A. Krozer, B. Kasemo, J. Less-Common Met. 152 (1989) 295–309.
[12] A.J. Du, S.C. Smith, X.D. Yao, G.Q. Lu, J. Am. Chem. Soc. 129 (2007) 10201–10204.
[13] A. Leon, E.J. Knystautas, J. Huot, S. Lo Russo, C.H. Koch, R. Schulz, J. Alloys Compd. 356 (2003) 530–535.
[14] N. Bazzanella, R. Checchetto, A. Miotello, Appl. Phys. Lett. 85 (2004) 5212–5214.
[15] K. Higuchi, H. Kajioka, K. Toiyama, H. Fujii, S. Orimo, Y. Kikuchi, J. Alloys Compd. 293–295 (1999) 484–489.
[16] J. Qu, Y. Wang, L. Xie, J. Zheng, Y. Liu, X. Li, Int. J. Hydrogen Energy 34 (2009) 1910–1915.
[17] J.N. Huiberts, R. Griessen, J.H. Rector, R.J. Wijngaarden, J.P. Dekker, D.G. de Groot, N.J. Koeman, Nature 380 (1996) 231–234.
[18] T.J. Richardson, J.L. Slack, R.D. Armitage, R. Kostecki, B. Farangis, M.D. Rubin, Appl. Phys. Lett. 78 (2001) 3047–3049.

[19] S. Bao, K. Tajima, Y. Yamada, M. Okada, K. Yoshimura, Appl. Phys. A-Mater. Sci. Process 87 (2007) 621–624.
[20] K. Yoshimura, Y. Yamada, M. Okada, Appl. Phys. Lett. 81 (2002) 4709–4711.
[21] A. Baldi, D.M. Borsa, H. Schreuders, J.H. Rector, T. Atmakidis, M. Bakker, H.A. Zondag, W.G.J. van Helden, B. Dam, R. Griessen, Int. J. Hydrogen Energy 33 (2008) 3188–3192.
[22] K. Yoshimura, S. Nakano, S. Uchinashi, S. Yamaura, H. Kimura, A. Inoue, Meas. Sci. Technol. 18 (2007) 3335–3338.
[23] S. Bao, K. Tajima, Y. Yamada, M. Okada, K. Yoshimura, Sol. Energy Mater. Sol. C 92 (2008) 224–227.
[24] K. Tajima, Y. Yamada, S. Bao, M. Okada, K. Yoshimura, Appl. Phys. Lett. 92 (2008) 041912.
[25] A. Borgschulte, R. Gremaud, S. de Man, R.J. Westerwaal, J.H. Rector, B. Dam, R. Griessen, Appl. Surf. Sci. 253 (2006) 1417–1423.
[26] K. Tajima, Y. Yamada, S. Bao, M. Okada, K. Yoshimura, J. Appl. Phys. 103 (2008) 013512.
[27] M. Pasturel, M. Slaman, H. Schreuders, J.H. Rector, D.M. Borsa, B. Dam, R. Griessen, J. Appl. Phys. 100 (2006) 023515.
[28] M. Avrami, J. Chem. Phys. 9 (1941) 177–184.
[29] J.F. Fernandez, C.R. Sanchez, J. Alloys Compd. 340 (2002) 189–198.
[30] J. Qu, Y. Wang, L. Xie, J. Zheng, Y. Liu, X. Li, J. Power Sources 186 (2009) 515–520.
[31] P. Hjort, A. Krozer, B. Kasemo, J. Alloys Compd. 234 (1996) L11–L15.
[32] R. Checchetto, N. Bazzanella, A. Miotello, P. Mengucci, J. Alloys Compd. 446 (2007) 58–62.
[33] A. Krozer, B. Kasemo, J. Less-Common Met. 160 (1990) 323–342.
[34] H. Hagi, Mater. Trans. JIM 31 (1990) 954–958.
[35] L. Yang, C. Yang-Tse, Int. J. Hydrogen Energy 21 (1996) 281–291.
[36] P. Spatz, H.A. Aebischer, A. Krozer, L. Schlapbach, Z. Phys. Chemie-Int. J. Res. Phys. Chem. Chem. Phys. 181 (1993) 393–397.
[37] S. Bao, Y. Yamada, M. Okada, K. Yoshimura, Appl. Surf. Sci. 253 (2007) 6268–6272.
[38] K. Tajima, Y. Yamada, S. Bao, M. Okada, K. Yoshimura, Appl. Phys. Lett. 91 (2007) 051908.
[39] T.J. Richardson, J.L. Slack, J.C.W. Locke, S. Seung-Wan, J. Ona. Sol. Energ. Mater. Sol. C 90 (2006) 485–490.
[40] A. Borgschulte, M. Rode, A. Jacob, J. Schoenes, J. Appl. Phys. 90 (2001) 1147–1154.
[41] A. Borgschulte, R.J. Westerwaal, J.H. Rector, B. Dam, R. Griessen, J. Schoenes, Phys. Rev. B 70 (2004) 155414.
[42] A. Fischer, H. Kostler, L. Schlapbach, J. Less-Common Met. 172 (1991) 808–815.